

Characterization and real-time removal of motion artifacts from EEG signals

Atila Kilicarslan¹, Jose Luis Contreras Vidal¹

¹ Department Electrical and Computer Engineering, University of Houston, Houston/TX, USA

E-mail: akilica2@central.uh.edu, JLContreras-Vidal@uh.edu

Received xxxxxx
Accepted for publication xxxxxx
Published xxxxxx

Abstract

Objective: Accurate implementation of real-time non-invasive Brain-Machine / Computer Interfaces (BMI / BCI) requires handling physiological and nonphysiological artifacts associated with the measurement modalities. For example, scalp electroencephalographic (EEG) measurements are often considered prone to excessive motion artifacts and other types of artifacts that contaminate the EEG recordings. Although the magnitude of such artifacts heavily depends on the task and the setup, complete minimization or isolation of such artifacts is generally not possible.

Approach: We present an adaptive de-noising framework with robustness properties, using a Volterra based non-linear mapping to characterize and handle the motion artifact contamination in EEG measurements. We asked healthy able-bodied subjects to walk on a treadmill at gait speeds of 1-to-4 mph, while we tracked the motion of select EEG electrodes with an infrared video-based motion tracking system. We also placed Inertial Measurement Unit (IMU) sensors on the forehead and feet of the subjects for assessing the overall head movement and segmenting the gait.

Main Results: We discuss in detail the characteristics of the motion artifacts and propose a real-time compatible solution to filter them. We report the effective handling of both the fundamental frequency of contamination (synchronized to the walking speed) and its harmonics. Event-Related Spectral Perturbation (ERSP) analysis for walking shows that the gait dependency of artifact contamination is also eliminated on all target frequencies.

Significance: The real-time compatibility and generalizability of our adaptive filtering framework allows for the effective use of non-invasive BMI/BCI systems and greatly expands the implementation type and application domains to other types of problems where signal denoising is desirable. Combined with our previous efforts of filtering ocular artifacts, the presented technique allows for a comprehensive adaptive filtering framework to increase the EEG Signal to Noise Ratio (SNR). We believe the implementation will benefit all non-invasive neural measurement modalities, including studies discussing neural correlates of movement and other internal states, not necessarily of BMI focus.

Keywords: EEG, real-time artifact removal, motion artifacts, ocular artifacts

1. Introduction

Investigating the neural sources, neural correlates and sensor domain connectivity/causality applications of human movement is of interest to many research areas including rehabilitation, restoration of movement of people with paralysis, or purely characterization studies assessing brain dynamics. Movement-related artifacts (or motion artifacts) are perhaps one of the most challenging non-physiological source of noises to handle, which can hinder the true performance of neural interfaces and the brain-machine interface (BMI) decoders, or skew offline results related to the sensor domain

analyses. Depending on the context of the data collection paradigm and the experimental setup, motion artifacts can manifest themselves continuously or partially whenever a head movement causes the electrodes to move with respect to the scalp. It is impossible to conclude, without further analysis of each experimental modality, whether or not the motion artifacts are present. The determination of the contaminants' existence and severity is highly dependent on the study in question. Researchers find it exceedingly difficult to conclude if the captured neural oscillations are simply due to electrode movement, or they are neural in origin. Even more challenging to answer is if there is a combination of both neural and

artifact-induced oscillations (linear or nonlinear), affecting also the observed phase and amplitude of the measured data.

In scalp electroencephalography (EEG) studies, there are ways to reduce or perhaps eliminate the movement related artifacts, by reducing or eliminating the relative EEG electrode movement w.r.t. the EEG cap, or scalp. In mobile brain-body imaging (MoBI) recordings, it is a good practice to use an external stabilizing layer on top of the EEG cap, such as a medical mesh. This would prevent the transmission of the overall cable bundle/cap inertia to the individual sensors, up to some level. Naturally, slow movements contain less or negligible artifactual components [1]. For other more dynamic applications (such as a fast walk/jogging or sudden head movements), the movement caused by inertia or cable pulls would simply be impossible to avoid. Fast head movements are also known to cause harmonics of the major contamination frequency, making the overall artifactual components exceedingly difficult to handle.

There are research efforts towards characterization of motion artifacts. A clear consensus among research groups is that the motion artifacts are highly dynamic in nature, and are affected by the setup and movement dynamics. It is also highly variable among subjects, within the same session and w.r.t. the scalp spatial location of EEG sensors [1]–[3] of the same subjects. However, there is still no consensus on how to handle these artifacts when they manifest themselves, how to characterize their conditional variabilities, and perhaps even less examined, how to remove/suppress them in *real-time*. In a recent study, researchers used a phantom head and a moving platform to induce and later separate the motion artifacts to simulated EEG dipoles. They showed that offline ICA analysis, even under the influence of motion artifacts gives meaningful dipole locations, which is of great importance for analyses that investigate neural dynamics in such a manner [4]. The use of phantom head equipped with EEG sensors has merit in identifying and testing solutions for motion artifact problem. Another study from the same group investigated motion artifacts as a result of the treadmill walking (at different speeds) [3]. They used a multi-layer cap where the neural signals were isolated from the electrodes to make sure the only remaining oscillatory signals were induced by motion artifacts. With the help of a head acceleration sensor (placed on the forehead), they check the correlation of the isolated motion artifact signals to the head acceleration values. However, it should be noted that the acceleration values were not compensated for gravity, thus any tilt caused gravity components, other than on the vertical axis, would register as a variable signal component. This component's effect on the registered motion artifact signal is of course unknown, one could argue in favor of more correlation, or simply a component that could distort any linear mapping. The authors concluded that the overall linear mapping from acceleration values to the electrode motion artifacts paints an incomplete

picture, at times yielding low correlation values. Nevertheless, their findings also support the consensus on the dynamic variability of the motion artifacts. They also investigated the usability of methods for removing the artifacts based on a moving average, wavelet transform and the combination of the two, concluding that although some suppressions were reported, other methods need to be developed for effective handling of motion artifacts. In [5], they also show that the dipoles identified using ICA where the input is pure motion artifact data (isolated EEG cap) are represented 99% in non-neural volumetric locations. However, the remaining 1% was falsely identified as a neural source, which stresses the importance of finding effective motion artifact cleaning methods.

Since the cause of the artifacts is the movement of the head, and associated relative electrode movement w.r.t. the cap, one could argue that the position (rather than the acceleration) of the relative movement would yield very high (linear) correlation values to the EEG since any scalp-EEG sensor contact change would be a function of the 3D position change. This linearity assumption would be closer to the truth if we would consider an EEG cap with a single electrode attached to it, and that there is no complex dynamic interaction between the cable bundles of multi-electrode setups. Even if we could avoid this electrode-electrode interaction, the inertia caused by the whole cable bundle would translate to the electrodes as a relative motion, given the suitable head movement. The experiment reported in [6] discusses the effect of the cable sway in generating the motion artifacts, which was tested and shown to be true using a phantom head and motion platform setup. Furthermore, in [7], the authors discuss the capacitive arrangement of signal measurements from scalp to the EEG electrodes. Although the gel layer has a certain capacitance, the electrons flow between the gel and the electrode, and a half-cell (DC) potential is formed. The authors refer to the settling needed (a few minutes) for the electrochemical interaction between the electrode and the gel reaching steady-state. We can argue that levels of electrode movement can, in fact, disturb the steady-state DC characteristics, causing superimposed oscillatory signals. This is further discussed in chapter-6 of [8]. Change in the resistance and DC potential at the skin/electrolyte junction was identified as one of the causes of motion artifacts. The repetitive disturbance of the skin/electrolyte and electrolyte/metal (EEG sensor tip) junction brings the question of the needed settling dynamics, and whether or not the cumulative effect's linear representation is adequate.

Given the analyses conducted in the abovementioned literature and the observed behavior in this study, we find that neither the linear representation and analysis nor the linear removal methods can handle the motion artifacts with the needed accuracy.

Several methods have been proposed in the literature for the removal of motion artifacts. In [9], authors investigate the removal of artifacts induced by treadmill walking. They segment the data into gait cycles and create an artifact template by averaging 20 strides. They then linearly regress the template to the data in the least squares sense. The regressed data is then subtracted for an artifact-reduced EEG data. They also apply the same method to the Independent Components (IC) after AMICA decomposition. They report a meaningful reduction in motion artifacts, although also acknowledging that it is unknown why on some subject's data additional reduction of artifacts were observed when used also the IC based method, and why on others this reduction was not as expected. A possible reason for this could be the template's accuracy, its linear projection onto the EEG and highly dynamic (changing characteristics) of the artifacts not allowing a linearly scaled template to represent the phenomena fully. Not to mention averaging to generate a generalizable template would require a repetitive artifact, which in real-life would be hard to ensure as the artifacts can be discontinuous or short living, also varying from one gait cycle to the next. Another IC based method was reported in [2]. The authors use a template correlation method to identify and reject EEG channels and ICs. However, similar to the previously mentioned study, the assumption is that steady-pace walking creates cyclic artifacts throughout the recording. Another cleaning method based on IC decomposition is presented in [10]. The authors decompose the EEG data and manually remove the non-motion artifact contaminants using the PREP pipeline. They identify the motion artifact components by utilizing the head acceleration power spectra and calculating the deviation w.r.t. the no-motion baseline EEG. In [11], authors use a headband type EEG setup and measure the EEG in sync with the IMU data. They decompose both using ICA and check the similar components to be removed from the data using cross correlation. No real-time implementation has been reported in the abovementioned methods.

In [12], [13], the authors present a different approach. They implement their approach to dry contact EEG electrodes. The continuous measurement of electrode-tissue impedance was used as the information to reduce the motion artifacts. They also suggest that the prediction of motion artifacts in one electrode site can be improved by the electrode-tissue impedance measurements from other electrode sites. A multi-channel linear predictor is then used to identify the artifact as an additive component to the EEG signals, using the mean square error as the cost function. The authors report a substantial reduction of the artifacts. Although the implementation is for dry electrodes, it gives us clues regarding multi-input combined information and its applicability to represent individual channel artifacts. Using global events on the head (in that case, the global information

was derived by fusing spatially spread information), could enable us to employ proper techniques to map and adapt it to individual sensor channels, which we used for our current work.

Similar to the ICA decomposition approach, authors in [14] uses the Canonical Correlation Analysis (CCA, for blind source separation) of multi-dimensional signals. Their multidimensional signal is formed from a single channel EEG. They use Ensemble Empirical Mode Decomposition to decompose the contents of the signal and run the CCA to identify the artifactual components to be removed accordingly. As in any other blind source separation algorithm, the CCA (although works on second-order statistics), has also a generalizing tendency through the data statistics. Both ICA and CCA implementations lack on identifying changes in IC's as a function of time, which improves the likelihood of maintaining residual artifacts after cleaning. It should also be noted that long sections of data are needed to generate healthier statistics for an effective removal, which works against their applicability to real-time systems.

In [15] and especially in [16], the authors discuss the inclusion of adaptive filters to clean motion artifact signals from physiological data (for EEG and functional Near Infrared Spectroscopy - fNIRS). The methods discussed in the articles are heavily based on the L2 norm and linear in nature. Good discussions on the selection of reference signals for the adaptive filters are also presented in these sources. Adaptive filters provide the means to avoid the abovementioned problem of artifact generalization and to adapt to the changing characteristics of the artifacts. Our recent work on identifying, characterizing and removing the ocular artifacts employ a robust variation (H^∞ estimator) of linear adaptive filters [17]. We show the generalization tendency of the ICA to ocular artifact representation, and also compare the envelope of the adapted weights through our method, per channel, to the fixed ICA weights. The mean of our weight envelope closely follows the fixed ICA weights, but with the added capability of allowing fluctuations (adaptation) around the ICA level weights, in time-domain. This reduces the residual artifactual components on the cleaned data set. Not to mention that our method is applicable in real-time, which is critical for closed-loop neural interface applications such as neuroprostheses. For the motion artifact problem, however, the linear mapping of the reference signals to the motion artifact contaminated EEG is found to be insufficient as it lacks the complex dynamic representation. Therefore we employ a non-linear mapping of a reference signal to the individual EEG electrodes. The method uses global information related to the subjects' movement and finds a non-linear projection to the EEG data. Perhaps the most common of such non-linear representation of dynamic systems is the Volterra series expansion. We use a second order Volterra series and adapt the variable weights of the terms at each sample. In [18],

authors used a similar approach and employed a Volterra series with Recursive Least Square (RLS) adaptation algorithm for motion artifacts in Photoplethysmography, for heart rate estimation. Estimating the weights of a Volterra series is a widely used technique, also for physiological signals of many different types. However, researchers often choose RLS or Least Mean Square (LMS) methods as an adaptation scheme. As mentioned above, the H^∞ estimator has the advantage of being robust to external disturbances, with guaranteed robustness properties within given bounds. There are multiple variations of the H^∞ filtering method. Most celebrated are the fixed and exponentially-weighted assumptions. The general usage of combined Volterra series and H^∞ filtering with exponential weight assumption (V- H^∞ /exp) was discussed in [19]. The author investigates the performance of the V- H^∞ /exp and compares it to Volterra RLS (V-RLS) and Volterra normalized LMS (V-nLMS). For time-varying environments with colored inputs, the transient performance of the V- H^∞ surpasses those of the V-RLS and V-nLMS. Similarly, the performance of the V- H^∞ /exp is high for steady-state and also for non-stationary signals.

Enhanced with the Volterra series expansion, we use the time-varying weight assumption for the H^∞ filter (as opposed to the exponential assumption as formulated in [19]). To enhance our method's accuracy for the harmonics of the fundamental movement frequency, we employ a framework that can identify all major contamination frequencies by creating the narrow-band filter-banked version of our reference signal and handle all target contamination frequencies of the EEG in a cascade filtering method (Figure 3).

In section 2, we discuss our data collection modality for characterizing and removing motion artifacts. We revisit our ocular artifact cleaning method and expand it for the motion artifact cleaning problem. Our combined ocular and motion artifact cleaning framework forms a real-time capable method for neural signal denoising. In section 3, we discuss the characteristics of the motion artifacts using select EEG channels, as well as scalp distribution statistics for all electrodes. We also discuss comparative results for time and frequency domain analysis, before and after artifact cleaning. To the best of our knowledge, this paper presents the most comprehensive characterization of motion artifacts during treadmill walking.

2. Materials and methods

2.1 Subjects, tasks, and measurements

Eleven (11) healthy able-bodied adults with no known gait deficiencies participated in this study after giving informed consent. All procedures were approved by the Institutional Review Board of the University of Houston.



Figure 1: Setup for the movement data collection. The treadmill was surrounded by a motion tracking system, for which the approximate capture area was limited to the head of each subject. Cameras were calibrated before each session.

Subjects were asked to walk on a treadmill (Figure 1) at 1-to-4 mph gait speeds for 6 minutes continuously. Each task was started and ended with a 1-minute quiet standing as baseline periods. The walking area was surrounded with 12 OptiTrack motion capture cameras. The workspace of all the cameras was limited to the head of the subjects for increased resolution, resulting in a mean tracking error of 0.07mm.

All subjects were equipped with a 64 channel gel based EEG system (actiCAP, Brain Products GmbH) with active electrodes and 10-20 distribution. We have used the Brain Products MOVE system to wirelessly transmit the EEG data to the recording computer. In this setup, the cap electrodes are connected to a wireless transmitter, which sits on the participant's shoulder. Note that other wireless EEG systems attach the transmitter to the EEG electrode cap, most likely at the back of the head. However, wires still need to be routed from each electrode to the transmitter, thus causing potential motion artifacts. 4 scalp electrodes were relocated around the eyes of the subject to measure the ocular artifacts in bipolar configuration (TP10-TP9 for Vertical-EOG and PO10-PO9 for Horizontal-EOG, [17]). Peripheral electrodes FT9 and FT10 were moved to FPz (normally ground) and FCz (normally reference) locations accordingly for a denser scalp coverage. Reference and Ground electrodes were moved to the right and left ears, accordingly.

No external layer on EEG electrodes was used (i.e., a medical mesh), conforming also with the most standard implementation of this system. An external mesh, covering the electrodes is a standard setup item in our laboratory as it was found to dramatically reduce the motion of the electrodes and cable sway. For the scope of this work, however, a clear presence of motion artifacts was needed for us to be able to

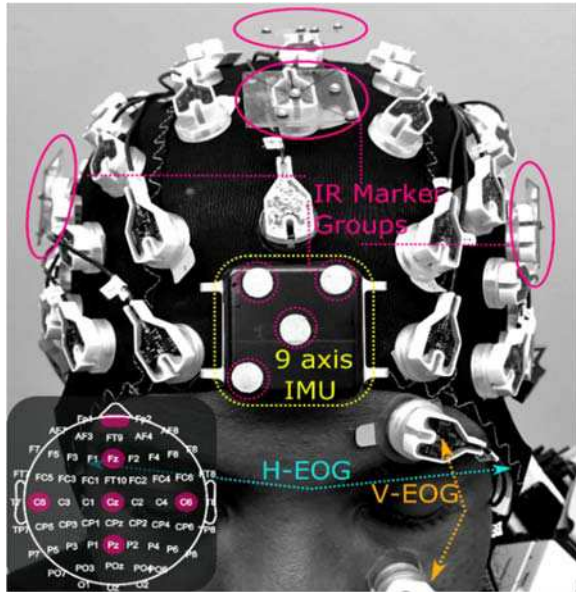


Figure 2: All subjects were equipped with a 64 channel EEG system, where 4 channels were assigned as bipolar horizontal and vertical EOG channels. A 9 axis IMU sensor was placed at the subject's forehead. Four infrared markers were placed on 5 selected electrodes.

characterize and assess the validity of our cleaning method (Figure 2).

All subjects were also equipped with 9-axis wireless IMU sensors (APDM, Opal), one at the forehead of the subjects, one on the right foot and one on the left foot. The forehead sensor was used to assess the usability of the IMU information to characterize and/or remove the motion artifacts. The sensors on the feet were used to segment the gait phases.

Five (5) of the select electrodes (Fz, Cz, Pz, C5, C6) were equipped with different reflective marker configurations for a precise measurement of the electrode cartesian positions, each containing 4 markers. Per sensor, markers were placed on a transparent plastic medium with < 1 gram weight and attached to the same sensor using the same orientation for all subjects (overall weight of the marker setup is ~0.8 [grams], per site). The surface of the forehead IMU sensor was also equipped with a reflective marker configuration (Figure 2). This information is used to derive velocity and acceleration data from the optically tracked position of the electrodes. We have used this information as a metric for a 2nd order standard Kalman filter implementation. The acceleration, derived from the Kalman filter (when the position is the only input) were compared with the IMU measured forehead acceleration and the error was used as a metric to optimize the error covariance matrix multiplier and the noise covariance values by forming a constrained optimization problem (Matlab *fmincon* function).

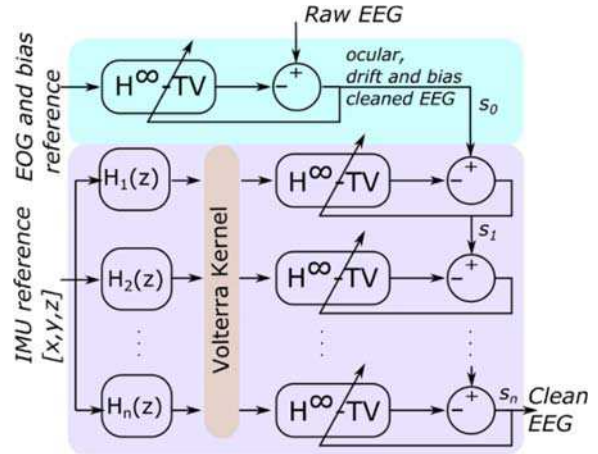


Figure 3: Joint Block Diagram for ocular and motion artifact removal from the raw EEG signal. The H^∞ adaptation rule is common for both tasks. A 2nd order Volterra series expansion was introduced per sub-band head movement reference for the motion artifact problem.

The EEG (fs=1000Hz), IMU (fs=128Hz), and OptiTrack (fs=120Hz) data were synchronized with a manually triggered logic signal at the run-time. All data were down-sampled to 100 Hz for analysis.

2.2 Combined ocular and motion artifact removal framework

As discussed in detail in [17], and summarized in section 2.2.1, our ocular artifact cleaning methodology is based on the robust H^∞ framework with time-varying weight formulation (H^∞ /TV). Both ocular artifact and the motion artifact cleaning methods use the same H^∞ adaptation rule, together forming a combined framework for real-time artifact handling. For the analysis in this paper, the EEG data were cleaned of ocular artifacts using the method summarized in section 2.2.1 prior to the motion artifact cleaning.

For the ocular artifacts, to accomplish a fast and effective cleaning, we have used a single weight value per reference input and estimated the weights with the H^∞ formulation, as:

$$d(i) = \mathbf{r}^T(i)\mathbf{w}(i) \\ = w_1(i) * eog_v(i) + w_2(i) * eog_h(i) + w_3(i) * 1 \quad (\text{eq. 1})$$

where $d(i)$ represents the unknown projection from the ocular artifact sources to the EEG channels for sample i , eog_v , eog_h are the vertical and horizontal EOG data and the constant 1 is used for the drift removal. Using this linear equation, we have shown the effectiveness of the robust-adaptive filter framework for the ocular artifacts, signal drift, and biases simultaneously in real-time. In the development stage of this work, we have found such a linear implementation only partially effective for the motion artifact problem, mainly

limited to the major frequency of contamination which is locked to the primary head movement frequency (Figure 8). To accomplish a better estimation of the head movement projection to each individual EEG channel, we introduced a 2nd order Volterra-series expansion of the reference inputs, having also 3 samples time taps. We also introduce a cascade filtering framework by implementing narrow filter banks for all target frequencies, including harmonics. The center frequencies of the filter bank were identified by the acceleration data frequency peaks. Figure 3 shows the combined structure of the adaptive filter implementation in this paper. It should be noted that the frequency bank includes all acceleration frequency peaks, regardless of their transmission to the measured EEG data. For the purposes of formulating a generalizable framework, it is left to our adaptive filter to identify the presence, level, and duration of the contamination per EEG channel.

The H^∞/TV formulation is revisited in the next sub-section as it applies to both the ocular artifacts and the motion artifact problem. The detailed discussion on the adaptation rule can be found in [17] and in [20].

2.2.1 The H^∞/TV adaptation rule

The performance of the sample adaptive filters depends on the type of the estimator used. Least-squares based estimators such as the Recursive Least Squares (RLS) or Kalman filter are maximum-likelihood and minimize the expected prediction error energy with the assumption of independent zero-mean Gaussian random variables and noise. This type of estimators are proposed in the literature for EEG signal processing [21], [22]. However, gaussian assumptions on random variables and noise processes remains a challenge for EEG signal processing. While estimating the weights (eq. 2), the H^∞ estimator provides guaranteed robustness properties for exogenous inputs within given bounds, where the gaussian noise process assumptions are also lifted.

The H^∞ adaptation rule with time-varying weight assumption is given as follows:

$$\hat{w}(i+1) = \hat{w}(i) + \frac{P(i)r(i)}{1+r^T(i)P(i)r(i)}y(i) \quad (\text{eq. 2})$$

$$d(i) = r^T(i)\hat{w}(i),$$

for which, $y(i) = s(i) - d(i)$,

$$\text{and } P^{-1}(i) = \tilde{P}^{-1}(i) - \gamma^{-2}r(i)r^T(i)$$

$$\text{where } \tilde{P}(i+1) = [\tilde{P}^{-1}(i) + (1 - \gamma^{-2})r(i)r^T(i)]^{-1} + qI$$

Here $\hat{w}(i)$ is the estimated weight vector of reference values, $r(i)$ is the reference vector at sample i , $s(i)$ represents the raw EEG data, and $y(i)$ is the clean EEG data. The parameters γ and q play an important role on the behavior of the adaptive filter. γ determine the bound on the energy-to-energy gain

from the disturbance to the estimation error, roughly determining the amount of disturbance that can be tolerated. For the time varying weight formulation, it should be selected as $\gamma > 1$. This defines a sub-optimal filter as a trade-off for allowing the weights to vary (although it's left to the user to tune the filter). The parameter q reflects the a priori information of how rapidly the weight will vary in time. Larger values covers for faster variations. For slow signals, $q \cong 10^{-8}$ is usually a good start point. It should be noted that these parameters can vary depending on the application in question.

2.2.2 Adaptive filter implementation for the motion artifact problem

Different from the ocular artifact cleaning method, for the motion artifacts, the non-linear variation of the reference projection is identified using eq. 2.

Volterra series modeling of the non-linear systems is a widely used approach in many disciplines. For the purpose of adaptive filtering, the series expansion allows us to use the linear adaptive filter formulations to adapt the weights assigned to each variable. A generic second-order Volterra series expansion is given in (eq. 3) [23]. The first term in (eq. 2) represents the weighted sum of the input with time lags and corresponds to the linear representation. The second term adds the weighted multiplication input instances at different lags and thus corresponds to the non-linear relationship. The adaptive filter identifies all weights of the representation of (eq. 2), yielding a more comprehensive coverage of underlying dynamics compared to identifying only the linear equation weights.

$$\begin{aligned} d(i) &= r^T(i)w(i) \\ &= \sum_{l_1=0}^N w_{l_1}(i)r(i-l_1) \\ &\quad + \sum_{l_1=0}^N \sum_{l_2=l_1}^N w_{l_1 l_2}(i)r(i-l_1)r(i-l_2) \end{aligned} \quad (\text{eq. 3})$$

Here $r(i)$ is the reference value used to identify the motion artifact projection. The terms $w_{l_1}(i)$ and $w_{l_1 l_2}(i)$ represents the Volterra kernel to be identified via the H^∞/TV adaptation rule and are identified using eq.2. For this implementation, the filter order is chosen as $N = 3$.

One very important aspect, apparently, is the selection of the reference signal that is used to identify the motion artifacts in EEG signals. We have used the 3-axis acceleration values, after gravity compensation using the quaternion of the IMU. For the gravity compensation, the acceleration vector values were converted to the earth coordinate frame using the quaternions, and then the gravitational vector values were

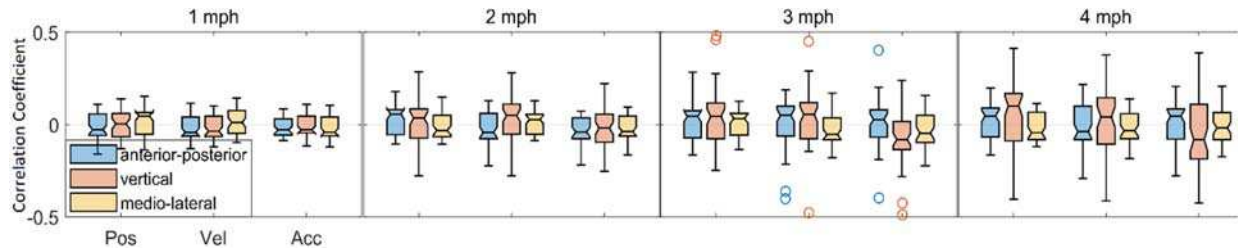


Figure 4: Group correlations for all subjects and marked electrodes for different walking speeds. Linear correlation is calculated between the EEG data and the individual sensors position, velocity and acceleration as measured and calculated by the motion capture system.

subtracted from the acceleration data. Our experimental setup allows us to use the individual electrode position, velocity and acceleration values as reference signals. The head IMU measurement is found to be adequate for removing the motion artifacts, as discussed and justified further in the subsequent sections.

After cleaning the ocular artifacts, we have used a zero-phase FIR filter in $[0.3 - 15]$ Hz range to bandpass filter the EEG data. Observed from their power spectrum (Figure 5), this range of EEG data is found to include all visible motion artifact harmonics. The discussion regarding the higher frequency level contamination is left for the discussion session. The data are then common average referenced, to be in parallel to previous literature work for comparison [3], [24]. Note that no other cleaning on the EEG data were performed prior to the motion artifact cleaning in order to assess the performance and selective nature (to motion artifacts) of our method.

3. Results

3.1 Non-linear properties of motion artifacts

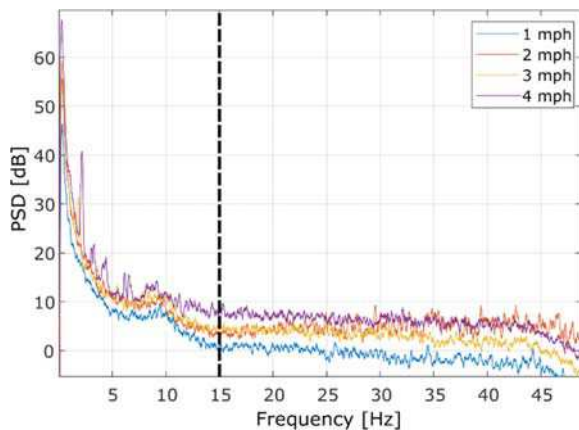


Figure 5: PSD grand average of all marked electrodes and subjects for different walking speeds. The major contamination peak and its harmonics become more dominant as the walking speed increases.

The application of linear correlation analysis alone to gauge the transmission of motion artifacts to EEG signals can hinder the true level of the artifact contamination. In a gel-based EEG setup, the disturbance caused by the movement between the skin-electrolyte and electrolyte-gel interfaces can be a repetitive action, manifesting the artifacts having repetitive transient dynamics [8]. Coupled with the electrode cable bundle and associated sway dynamics [6], we expect the projection of the artifact from the actual head kinematics to the EEG recordings to be inherently highly non-linear. We would also expect extensive differences on the projection levels of the motion artifacts for different electrode sites. The non-linearity and dynamic characteristics could be reduced to more manageable levels by the use of a head-mesh and limiting the cable sway, essentially coupling the electrodes mechanically. As such, considering the variability in EEG electrode systems and setups, a specific combination might yield a type of contamination that is more linearly dependent to the signal in question (i.e., the position, velocity, acceleration of the head). For the purpose of this study, we have retained from any application that could reduce the artifact contamination, and have used an EEG setup that is a standard implementation in conformity with the most generic EEG setups.

The linear correlation between measured quantities (position, velocity, and acceleration) and the EEG signals are summarized in Figure 4. We have grouped all subjects and all marked electrodes, and used the entire duration of the experiment to calculate the values. Signals are also shifted where applicable to yield the largest correlation values [3]. The correlation between the EEG data and the measured position of the individual electrode increases as the walking speed increases. In general, the faster speeds yield larger correlations, as well as larger correlation span in vertical movements. However, there are instances of larger median values in anterior-posterior and medio-lateral directions for various speeds and quantities. This shows the dynamic characteristics of the contamination and justifies the need for multi-axis reference signals for cleaning the EEG data. The velocity and acceleration derived from the measured position via a parameter optimized Kalman filter yield similar correlation values, but slightly less compared to the position

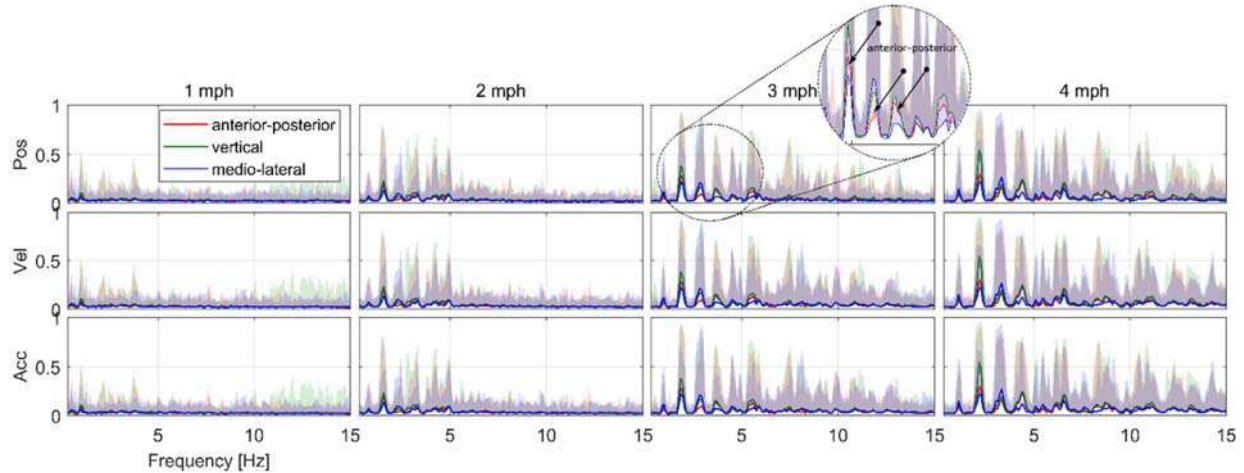


Figure 6: Group coherence for all subjects and marked electrodes for different walking speeds. The median values per axis are plotted as bold lines, and the variation around them for all subjects and electrodes were plotted as shaded regions. Note the high variance around the median frequency coherence.

of the same electrode. All EEG data are found to be both positively and inversely correlated with the sensor position, velocity and acceleration. The maximum median correlation value for the given quantities is around 0.1, whereas the overall maximum is ~ 0.4 . Having some level of correlation values should be investigated carefully. It should be remembered that the values reported are linear correlation between the EEG and the measured kinematic quantities. For complex problems such as motion artifact contamination and also considering the transient dynamics of the electrode-electrolyte and electrolyte-scalp layer disturbances, these values should not be regarded as the only representation of the interaction between the electrode and the measured quantities. Linear correlation, as the name suggests, assesses only the linear part of a complex interaction. The linear part, in this context, can only model/characterize the local linear behaviour, or the linear components of an overall non-linear equation. As such, although the values increase with the increasing walking speed, these values should not be taken as the final and full assessment of the contamination level and type. From the linear correlation perspective, these correlation values suggest minimal-to-medium motion artifact contamination. However, the frequency domain analysis paints a different picture. Figure 5 shows the grand average PSD of EEG data from all marked electrodes, for all subjects and 2 minutes of continuous walking. Although the spectral motion contamination is inconclusive at the grand average level for the slow walking speed of 1 mph, at higher speeds, the contamination is apparent, exhibiting also strong harmonics. Checking the frequency coherence of the EEG to the EEG electrode kinematics (position, velocity, and acceleration of the individual EEG sensor) supports the idea of strong contamination in higher speeds. Figure 6

summarizes the grand average coherence values for all marked electrodes and all subjects. The solid lines represent the mean coherence per axis of motion, and the shaded regions represent the variance around it. As expected, higher walking speeds result in higher coherence values. The differences between position, velocity, and acceleration based synchrony are harder to see in a coherence plot and all quantities exhibit similar frequency peaks and harmonics.

One interesting finding is the characteristics of coherence peaks at different harmonics. In general, all 3 axes (anterior-posterior, vertical and medio-lateral) of electrode movements yield strong harmonics, the vertical axis usually being the strongest. However, some harmonics appear to be majorly generated by only one or two of the axes. The inset in Figure 6 details the subsequent harmonics' contributions per axis, showing that the 2nd peak is strongly correlated with the medio-lateral and vertical axes, whereas the contribution of the anterior-posterior movement is less compared to the two. The 3rd peak, however, is mostly affected by the vertical and anterior-posterior axes and the medio-lateral axis contributes less. We assume this to be caused by the different filtering effects generated by the electrode setup/cable dynamics, since some frequencies in the same axes are damped, whereas subsequent higher frequency dynamics are not. This is not always the case for different walking speeds, electrode locations and subjects, hence, there is no generalizable way of representing the higher order nonlinearities of such a complex problem. Furthermore, the existence of high amplitude frequency locked components in EEG data (spanning almost 25 dB range in high walking speeds, Figure 5), and loosely correlated time domain data to the position, velocity, and acceleration of the specific EEG sensor suggests a complex non-linear relation between the electrode kinematics and the

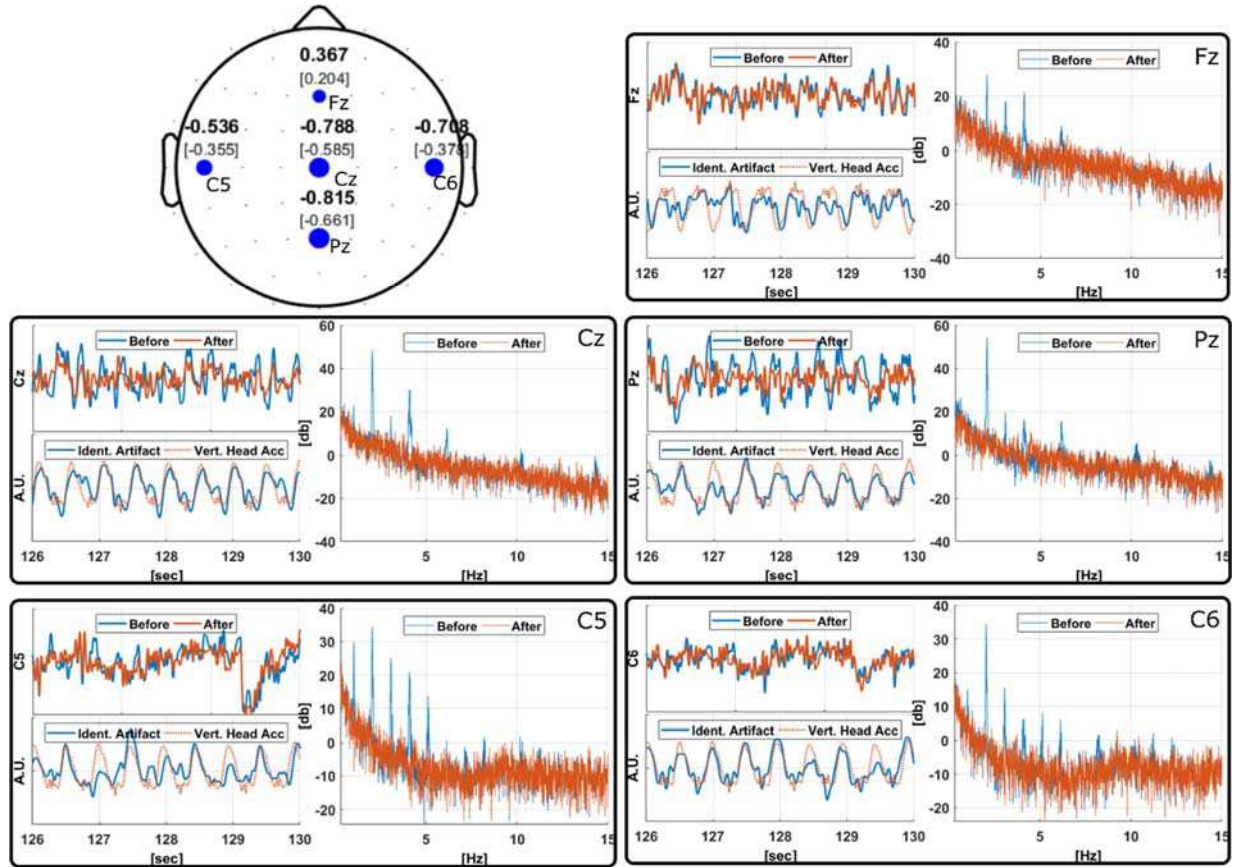


Figure 7: Identified artifacts and their properties. Scalp values show the linear correlation values between the identified artifact and the vertical forehead acceleration for sensors equipped with the motion tracking markers (full session data – 6 minutes). The values in brackets show the values for the raw EEG and same vertical acceleration for comparison. Each panel of plots show the before/after filtering of the motion artifacts for continuous 4 seconds of data for visibility (upper left), the identified artifact of the specific channel and the vertical forehead acceleration for the whole duration of the experiment (6 minutes) (bottom-left), and the power spectrum of the raw EEG and the motion artifact filtered EEG for the whole duration of the experiment (6 minutes) (right).

projected contamination. Therefore, for a conclusive test of whether or not the EEG is under the influence of motion artifacts, and if there is contamination, the level and time domain characteristics and even the discrete vs continuous existence should be investigated by methods that allow for a sample-by-sample non-linear mapping. This essentially suggests identification of the artifactual components in the time domain. We investigate the applicability of identifying the nonlinear representation (Volterra Kernel coefficients) through a sample adaptive filter to characterize the motion artifacts. This sample-by-sample adaptation, contrary to the statistical methods, can not only tell us of the existence of motion artifacts at different instances within a session, but it can also help us define the abovementioned characteristics.

3.2 Removal of motion artifacts

To test the effectiveness of our method, we have used all marked electrodes' (Fz, Cz, Pz, C5, C6) positions, captured by

the OptiTrack motion capture system for 4 [mph] walking speed. The fastest walking speed is chosen to ensure the presence and in fact dominance of motion artifacts. For our offline analysis, the availability of this detailed information is valuable in understanding the motion artifact components of the measured signals. However, for a wide-scale application, this information is unlikely to be available, thus we seek to understand the characteristics of the artifacts and determine if another measurement modality can be used instead of the precise electrode position. The position measurements provide us with the oscillatory (regardless of the artifact being continuous or intermittent) electrode dynamics, which is technically the main cause of the artifacts (electrode position shift causing the disturbance in the skin/electrolyte and electrolyte/metal interfaces). To identify the fundamental and harmonic frequencies of the contaminating movement with peak spectral power, the movement signal is spectrally whitened and the peaks were identified. This whitening is done to automate the detection of the spectral peaks with

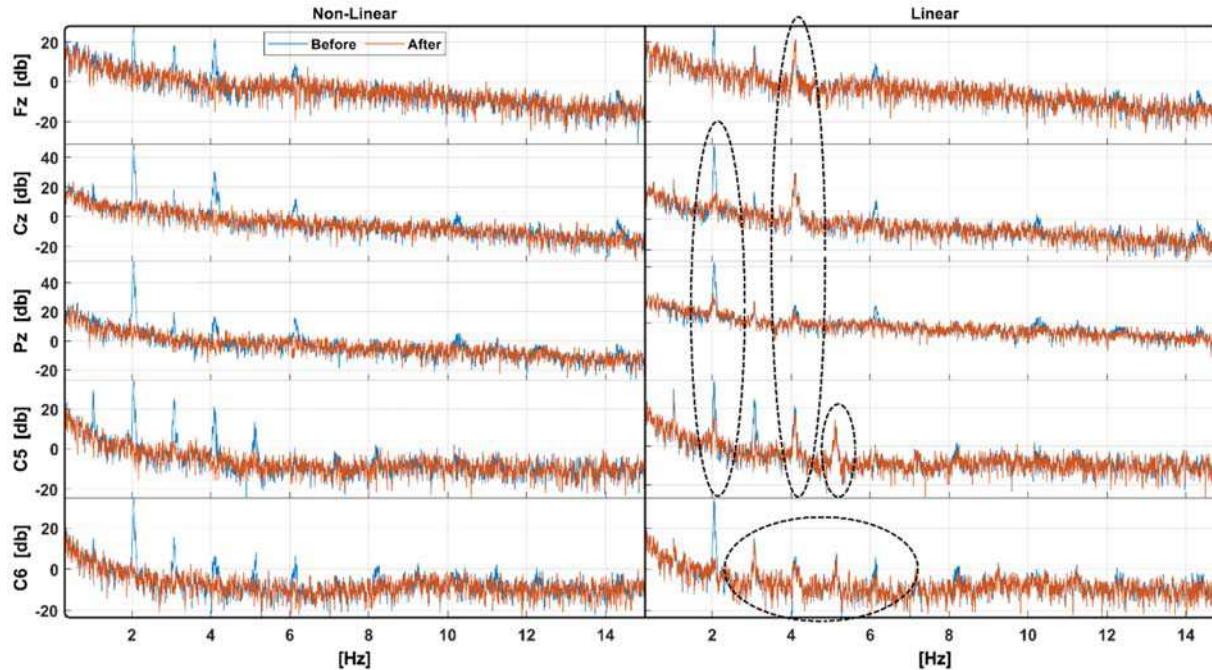


Figure 8: Comparison of the PSDs using a linear and non-linear filter to clean motion artifacts for a subject with 4mph walking speed. Linear adaptive filter implementation has the same parameters as the non-linear adaptive filter, only lacking the non-linear Volterra Kernel representation. Notable shortcomings were circled where the artifact suppression is inadequate when using the linear filter.

improved accuracy. The reference signal is then bandpass filtered to each of the identified frequencies f_j ($j = 1, \dots, n$), where n is the number of frequency peaks. The passband boundaries are selected as $[f_j - 0.6, f_j + 0.6]$ Hz. The reference signals were then passed to the Volterra series representation to create a non-linear representation. The weights were then identified using the H^∞ /TV formulation in a cascade manner where the input of the adaptive filtering process $j + 1$ is the output of process j .

The overall artifactual component in the EEG signal is then calculated as the difference between the raw and the final clean EEG data as: $a(i) = s(i) - y(i)$. The artifactual component $a(i)$ is then used to assess the characteristics of the motion artifacts.

Figure 7 summarizes the findings for the sensors of interest when the *cartesian positions* of the electrodes were used to identify the artifactual components. The identified components were also compared to the vertical axis of the head acceleration measured by the head IMU sensor for 4 mph walking speed (on average, the vertical axis correlates most for this walking speed as shown in Figure 4). The reported linear correlation values between the vertical head acceleration and the identified artifacts were calculated by shifting the signals, when needed, to yield the maximum correlation. The data point shifts are within $50 - t_0 -$

$90[ms]$ (5-to-9 samples). Figure 7 top left scalp plot reports these correlation values for the select electrodes. Each panel of plots show a short segment of signal (for visibility) of raw and clean EEG (top-left), identified artifact and the vertical head acceleration (bottom-left), and the power spectrums of raw and cleaned EEG signals (right, for the full data set, 6 minutes of recording). Note that the identified artifact vs. head acceleration plot changes the sign of the identified artifact for providing better visibility in the level of correlation. First to notice is the sharp peaks in the power spectra plots, where the frequency is locked to the head movement/walking speed, and its harmonics. The overlaid clean EEG power spectrum show a clear suppression on the major contamination frequency and all of its harmonics. This not only shows the effectiveness of the method, but also clearly indicates the selective nature of the cleaning paradigm. The spectral details where the artifact peaks are not visible are an exact match between the raw and cleaned EEG signals. Also, time domain EEG amplitude modulation based features are preserved, while only the artifactual components of the signal are cleaned. As an example, note that the C5 electrode raw signal time domain amplitude dip ($\sim 129^{\text{th}}$ second) is perfectly preserved, while other amplitude changes, identified as artifactual components in the more steady-state section of the data are removed. Of course, the keyword -time domain feature- used here does not necessarily limit to the task

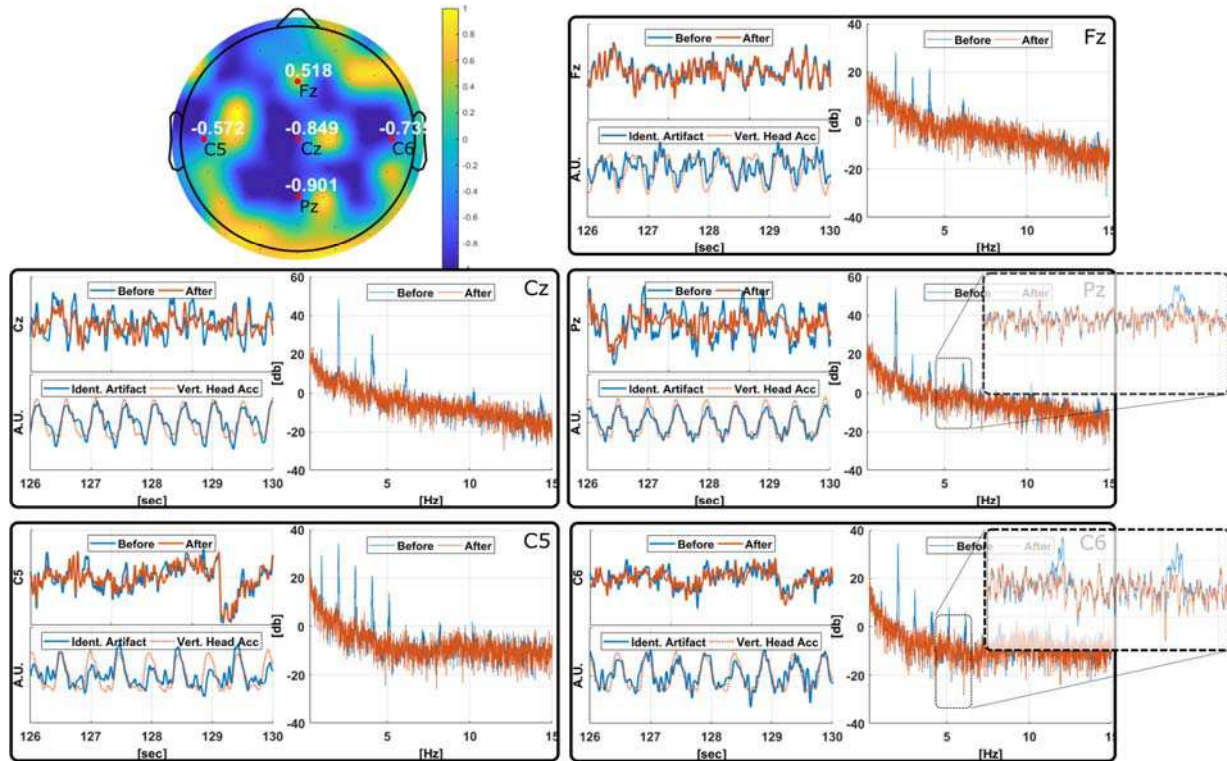


Figure 9: Identified artifacts when the reference signal is the 3-axis gravity compensated acceleration values. The scalp values show the linear correlation between the identified artifactual signal and the vertical head acceleration. Note the possibility of visualizing values for the entire scalp contamination. Each panel of plots, for select electrodes, show the raw and clean EEG signal segment (upper-left), identified artifact and the vertical head acceleration segment (lower-left) and the power spectra of the raw and clean EEG for the entire data-set (right).

dependent cortical oscillations and associated amplitude modulations. It rather points to the fine details of an EEG signal's characteristics, and their preservation by our method during motion artifact cleaning of a heavily contaminated EEG signal. One striking observation is that the time domain modulation of the identified artifact signals closely resemble vertical head acceleration values measured simultaneously with the EEG. To summarize the significance: the precise measurement of the position of each electrode was mapped via a nonlinear transformation to the measured EEG signals. These final position projections were then linearly correlated to the IMU measured head acceleration signals. It's found that the identified nonlinear transformation yield high *linear* correlation values compared with the acceleration sensor data. The linear correlation between the raw EEG and the head acceleration, without any processing, was found to be small (indicated as bracketed values on the scalp plot), compared to what has been transformed from the position data. An acceleration sensor is a very low-cost device which is already an integral part of many commercial EEG systems. Thus, accessing the synchronized acceleration data from any of those systems poses no difficulties. Even systems without the

acceleration sensors can be used by placing an external sensor to the forehead of the subject and synchronizing the data with the EEG signals, as has been done in this study. The high linear correlation between these quantities is a promising prospect to use the acceleration values for a sample-by-sample, real-time cleaning of EEG signal from motion artifacts. One very important property of using the forehead acceleration (IMU) sensor measurements as a reference signal is that it allows for filtering the entire scalp EEG locations. since the values reported are linear correlations, we can conclude with high level of confidence that the usage of acceleration sensor values as a reference input to the adaptive noise canceller is feasible. The projection of the forehead acceleration values, via our non-linear method, to identify a projection that is already highly linearly correlated with the acceleration values should yield similar or better results.

Another observation, confirming the literature on movement artifact removal methods as discussed in the introduction section, is the variability of the identified artifacts by channel locations. The contamination levels (as judged by the spectral peaks and harmonics) are also variable by sensor location as expected. The time domain characteristics of a

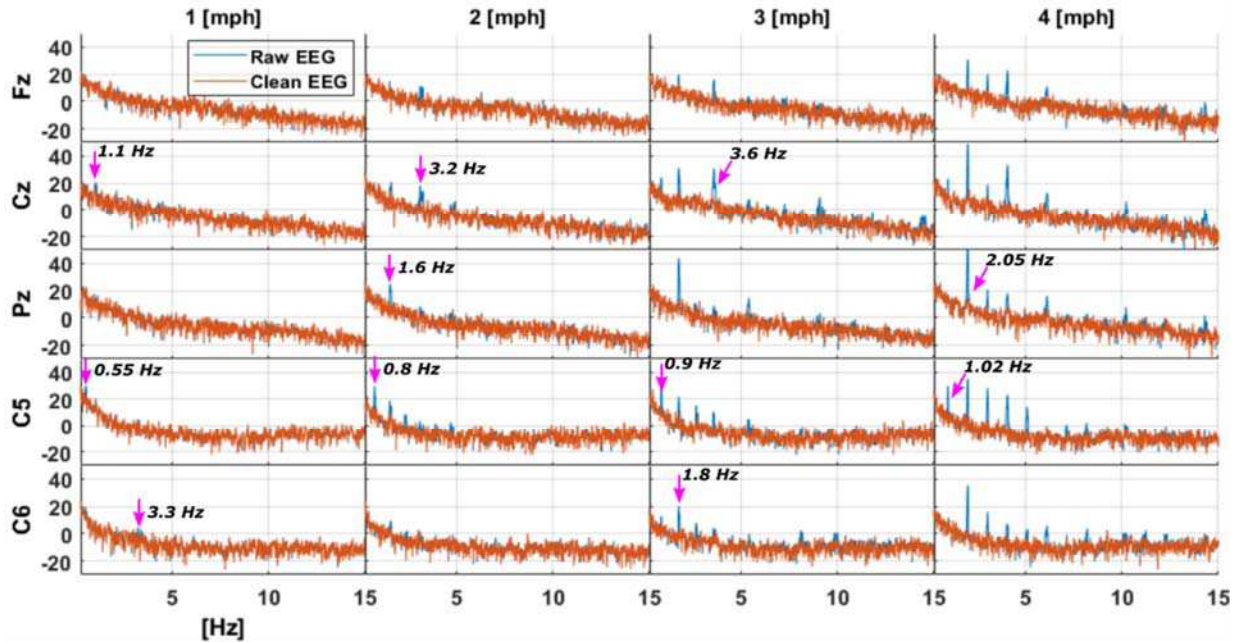


Figure 10: Power spectra of the raw and clean EEG signals for select electrodes and all experimental conditions. Some prominent harmonics were marked to show the variability of the artifacts and the selective nature of our time-domain cleaning method per condition and channel.

single channel artifact within the same recording session also show variability. Sample adaptive formulations in this sense allow us to identify informed projections with varying levels of contamination in time domain.

Our next step is to justify the usage of the acceleration data as a reference input. We have used all 3-axis head acceleration values (measured by the forehead IMU and gravity compensated) as reference signals to our algorithm and compare the cleaning performance and linear correlation values. Figure 9 scalp topographical plot shows the distribution of how well the identified artifact signal, per electrode, is related to the head acceleration values via linear correlation. Compared to the position reference signal for cleaning, the linear correlation yields higher values for the marked electrodes. This supports the idea of using acceleration as a reference signal, not necessarily because it's by default correlated to the raw EEG, but because its time domain properties and information-rich structure are highly relevant to the motion artifact contamination, should a proper non-linear mapping technique is used for identification.

Another important property to notice is the irregular distribution of correlations among scalp locations. Apparently, as stated in the introduction, due to the high dynamic interaction between the cable bundle and the electrode, bundle sway and other factors that cause non-linear mapping, the contamination level, and correlation sign varies greatly for all scalp locations, and does not follow a clear distribution. The power spectral comparison of raw and clean EEG signals show a very effective cleaning process, which is

selective of individual signal contamination level. We would like to stress that the same reference signal and frequency bins were used for *all* scalp areas as a reference signal. Comparing the harmonic peaks appearances and the prominences, it is clear that each electrode experiences different non-linear contamination dynamics. As an example, the Cz raw signal peaks show a sparse distribution compared to say the C5 and C6 electrodes and the ~ 5 Hz harmonic peak is not visible in Cz, Fz or in Pz. Yet the robust adaptive nature of our algorithm is capable of identifying when there is a relevant peak and when there is not, keeping the frequency information in the signal intact, when needed (see the inset plots for C6 and Pz in Figure 9).

The above cleaning using the acceleration values as reference signals is repeated using the linear equivalent of our non-linear framework to further justify the needed rich non-linear filter representation. We have used the same H^∞ adaptation rule with the same parameters as in the non-linear case, but instead of using the Volterra kernel, we have used a linear combination of 3-axis acceleration values as reference signals:

$$d(i) = w_1(i) * acc_x(i) + w_2(i) * acc_y(i) + w_3(i) * acc_z \quad (\text{eq. 4})$$

Figure 8 shows the before and after cleaning power spectra for 5 marked electrodes for both linear and non-linear cases. Although most of the major contamination frequencies are

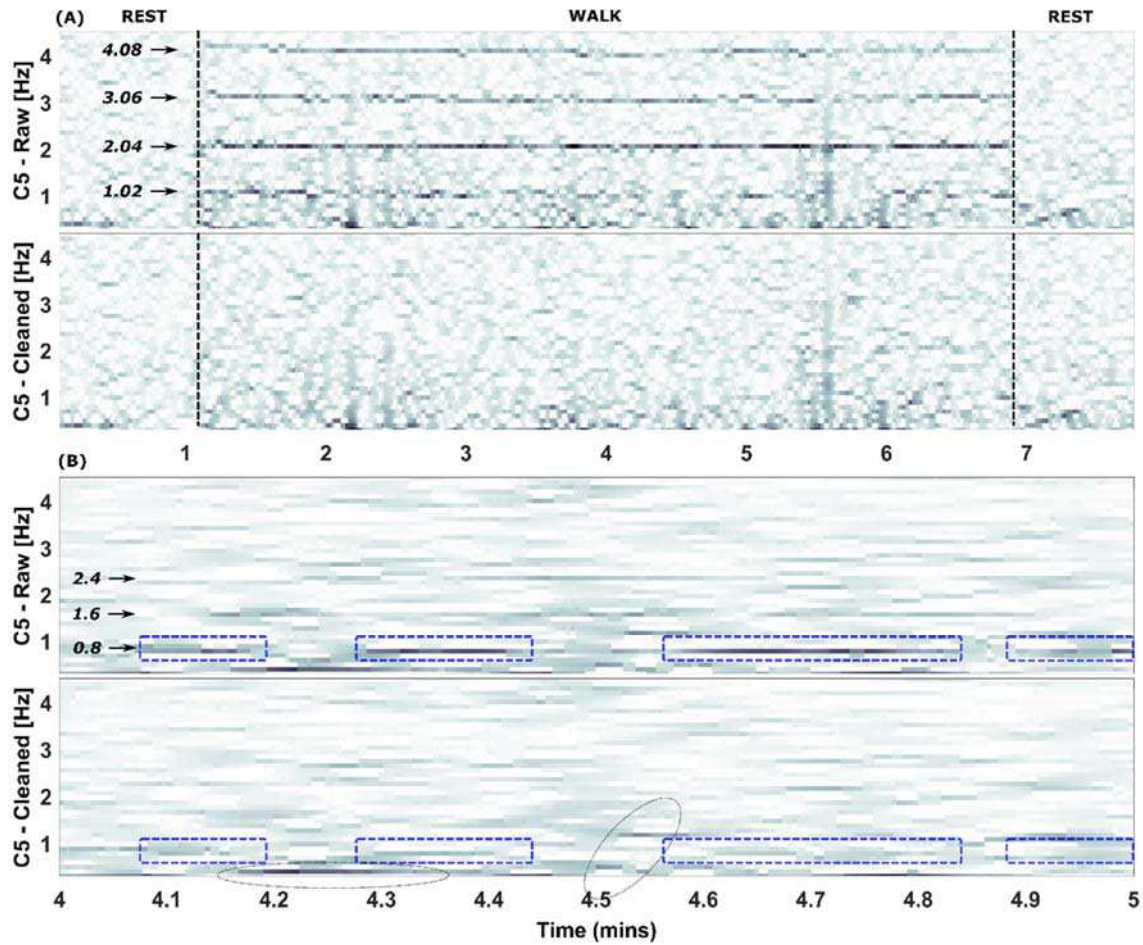


Figure 11: Time-frequency plot of delta band EEG data (C5 electrode): (A) 4mph walking speed and the entire duration of the experiment. Upper and lower plots show the data before and after motion artifact cleaning, respectively. Note the fundamental and harmonic frequencies before and after cleaning. (B) 2mph walking speed and 1-minute segment of data for visibility. 0.8 Hz

cleaned, some residuals remain in both major frequencies and their harmonics. Some notable residual artifacts were marked with black circles in the linear-case.

Finally, using the non-linear filter, we have also extended the results to all walking speeds for select electrodes (Figure 10) and compared the before/after cleaning power spectra. The variability of the artifact harmonics is also prominent in all walking conditions. Plots were generated for continuous 4 minutes of treadmill walking data. Note that the slower walking speeds (especially 1-mph) have far less artifact contamination. The clean EEG spectra do not show any clear sign of remaining artifacts. It should be noted that the presence of an artifact peak or harmonics does not necessarily mean the contamination for the entire experimental duration. Rather, what we have observed is that the artifacts, especially for slower speeds, manifest themselves in a discontinuous manner, showing stronger appearance at some sections and no apparent contamination on others. This is due to the discontinuous nature of the artifacts. It should be noted that,

although very slow walking speeds suggest less likelihood of electrode movements, we are concerned with any fast head movements, strong enough to generate artifacts. This also justifies the need for a cleaning method that can take into account artifacts with short duration, which may be statistically insignificant considering the full duration of the experiment. Figure 11 shows two sets of time-frequency plots that summarize the discontinuous appearances of the artifacts. Since the artifact dynamics are highly variable among subjects and electrode locations, a sample short segment of data was used to highlight the discontinuous nature of the artifacts. For the segment in Figure 11-B (2mph walking), the 0.8 Hz contamination is visible before cleaning the artifacts (upper plot). Within one minute of recording, 4 shorter segments of contaminations were observed. The cleaned time-frequency plot has no visible contamination at the same time instances. This plot also shows the selective nature of our cleaning method as the contaminated segments were cleaned (marked with boxes) and the rest of the time-frequency representation

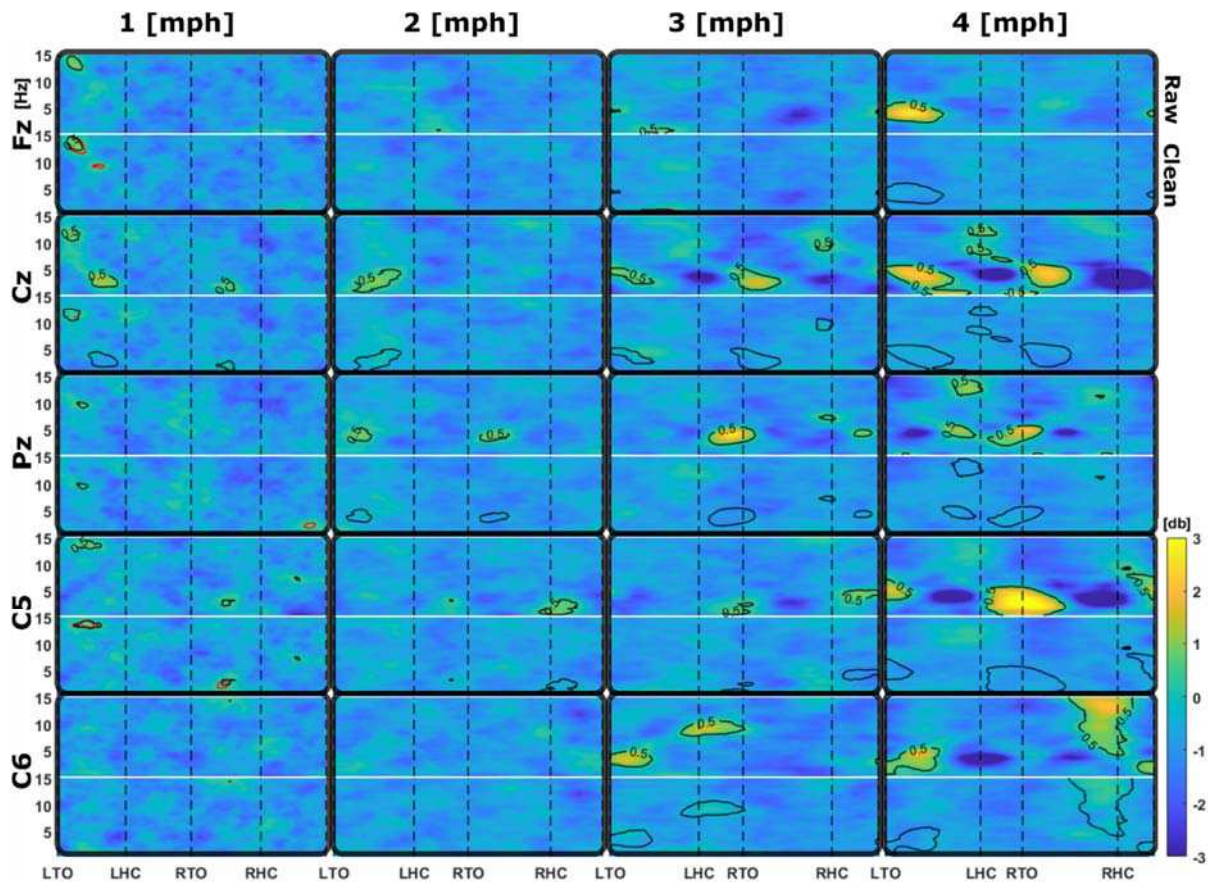


Figure 12: ERSP for the same subject and for all walking speeds and marked electrodes. Each panel, raw (upper) and cleaned (lower) data ERSPs are shown. LTO, LHC, RTO, and RHC are gait phases and refer to left toe off, left heel contact, right toe off and right heel contact, respectively.

remain intact where no apparent contamination harmonics were expected (some minor features preserved after cleaning were marked with circles). Figure 11-A shows the data from the entire duration of the experiment and for faster (4mph) walking speed. All fundamental and harmonic peaks of contamination were handled by our method (note also the wide spectrum non-motion artifact events at 2.1 and 5.5 minutes).

The variability of artifact appearance instances and dynamics prevents us from generating group statistics for a continuous, long segment time/frequency analysis, and gauge the performance of our algorithm. One way of accomplishing this is investigating the event dependent nature of the artifacts to rule out the cancellation of artifactual features on a grand average level. For a walking task, the Event-Related Spectral Perturbations (ERSP) analysis is a good way of determining the extent of our algorithm. Per subject and walking speed, we have calculated the time-frequency spectrum of EEG data from all scalp locations and segmented them with respect to the gait events. We have then

time warped the segments to the mean gait duration and excluded the gait durations that are of above or below 3 standard deviation of the mean gait duration.

Figure 12 shows the ERSP of all marked electrodes for the same subject to be able to compare the results with abovementioned outcomes for all 4 walking speeds. For each condition, the raw (upper) and cleaned (lower) data ERSPs were presented. We have marked the above 0.5 [db] contour lines found on the raw data ERSPs (black). Same contour lines for each condition were also plotted on ERSPs of the cleaned data for comparison. The red contour plots on the bottom ERSPs are specific to the cleaned data. As can be seen from the 1-mph walking condition, the raw data has gait locked events around 14 Hz range. However, checking the entire power spectrum of the same channel (Figure 10), 1mph walking has strong contamination for around 0.55 Hz, which is in parallel with the actual walking speed.

There is no evidence that these gait-locked power spectral changes for the 1-mph condition are representative of motion artifacts. Our algorithm keeps this information intact as can be seen from the cleaned data ERSPs and red >0.5 [db] contours.

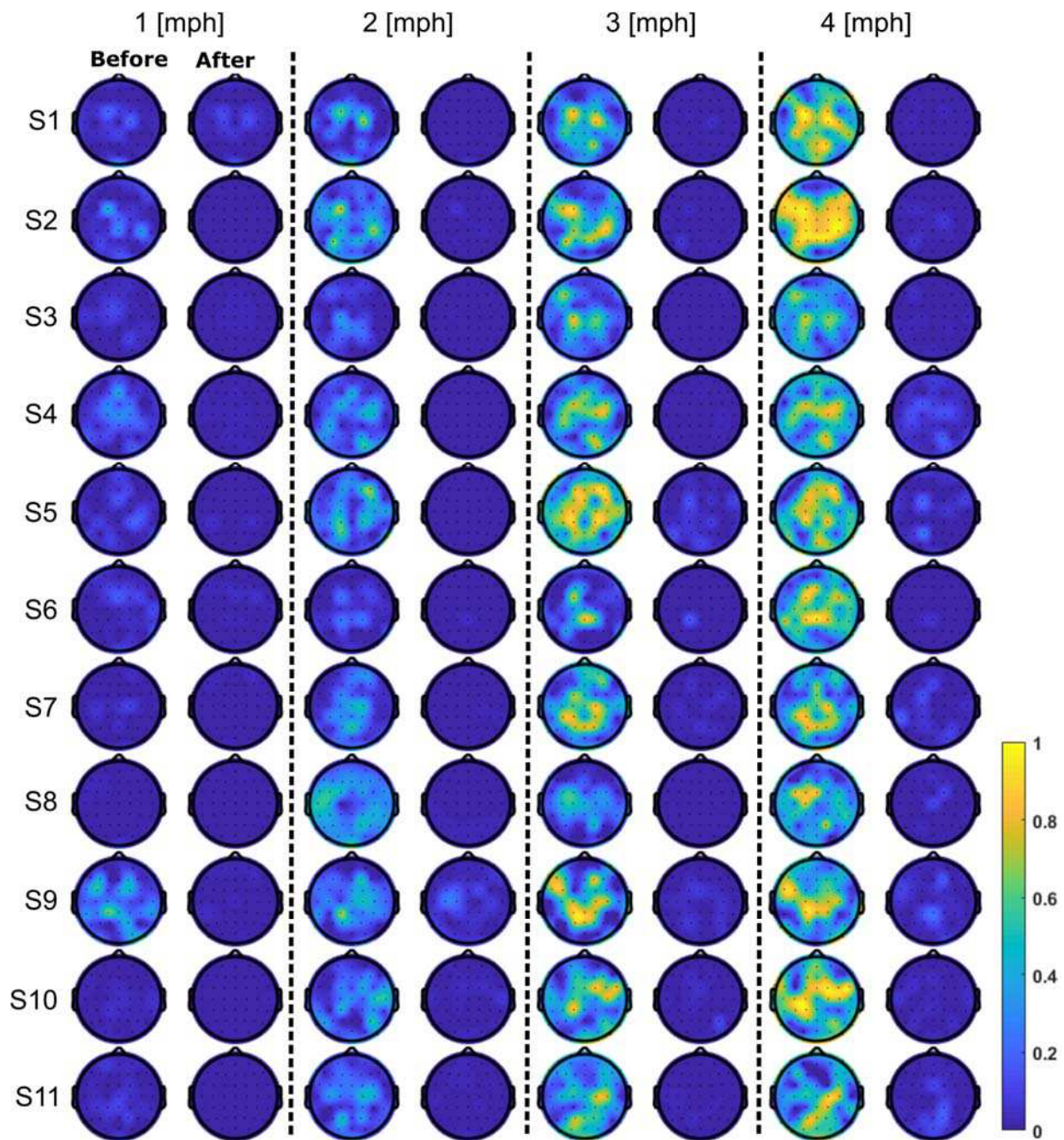


Figure 13: Coherence between all EEG electrodes and the forehead acceleration. Before and after motion artifact cleaning analyses were done for all subjects and all walking conditions.

The 2-mph condition, however, shows strong gait locked activity and the values are in the expected range for motion artifacts. Our algorithm marks this event as motion artifact and removes it effectively. Similarly, the 3-mph condition shows activity around the expected frequencies for motion artifacts. The activity for this walking speed becomes visible, especially for the LHC and RTO stages. In fact, ~ 5 Hz activity is also visible as a harmonic peak in Figure 10. Both the ~ 1 Hz and

~ 5 Hz activities were identified as motion artifacts and cleaned automatically by our algorithm. As expected, the gait locked activity increases with the walking speed. The 4-mph condition shows very strong activity in varying walking stages per electrode. Our algorithm was able to identify all occurrences as artifacts and effectively clean them. For better visibility of lower frequency cleaning performance, please refer to Supplementary Material-A. In Supplement-A Figure-

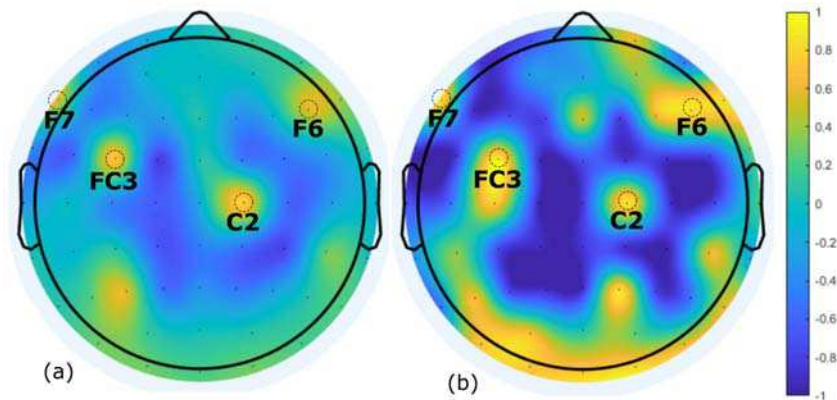


Figure 14: (a) Spearman correlation coefficient between vertical head acceleration and raw EEG. (b) Linear correlation coefficient between vertical head acceleration and identified artifacts (complementary to figure-9). Entire duration of the experiment was used while the subject walks on a treadmill at 4 mph speed.

1, the same ERSPs were plotted with logarithmic y-axis. All expected frequencies for all conditions were cleaned effectively. Note that in the Fz electrode -3mph walking condition, between LTO and LHC, the plot shows a 'blob' in the lower delta band frequencies that remained after denoising by our proposed algorithm. This implies that this neural activity is highly likely of a neural origin. Moreover, the algorithm cleaned all other target frequencies. Nevertheless, we caution the reader that there is a low likelihood that this unique delta activation in the Fz-3mph condition may be a leaked motion artifact. These examples can be extended to all scalp electrode locations, subjects and speeds as we do not bound our algorithm, or the input data to any electrode, subject, or condition-specific variable which are hard to measure. Instead, as justified before, the IMU data is found to be applicable for all conditions and scalp spatial locations. Although the time domain correlations are found to be inadequate to assess the true level of contamination, the frequency coherence values are found to be more informative when calculated w.r.t. the head acceleration values. To summarize the before/after coherences for all subjects and assess the effectiveness of the algorithm for all walking speeds and all scalp electrodes, we have calculated the coherence values of the major contamination frequencies per electrode. The area under the coherence curve for the major contamination frequencies were calculated for before and after cleaning conditions and divided by the number of frequency values for normalization. Figure 13 scalp topographical plots show the percentage coherence metric as an indicator of the motion artifact contamination for all subjects and walking speeds. The 4-mph speed, as expected, yields the highest average coherences across all scalp locations before cleaning. Although the slowest speed introduces the lowest values, the variability among subjects is apparent. As an example, the subject S9 experiences more artifacts compared to others for 1mph walking speed. This shows the variability of the artifacts even when the experimental conditions are the same among subjects.

4. Discussion

We have provided a comprehensive filtering framework for handling one of the most significant, and yet to be solved problem associated with all EEG recording paradigms, especially ones that require mobile tasks. Of course, the term mobile is used to represent any EEG recording session that results in head motion which causes motion artifacts. Our algorithms can be used as an offline post-processing tool for any recordings that provides a synchronized set of IMU sensor data with the EEG data. We have employed the acceleration data of the forehead IMU unit and compensated the gravitational acceleration using the quaternions derived from the gyroscope and magnetometer data. Although we could calculate the quaternions via many known and very well established methods, most IMU systems provide this information as an already calculated output signal, as in the APDM OPAL system used in this study.

One significant advantage of our method is its real-time applicability. Our method utilizes the IMU data and updates the parameters of the non-linear projection from the acceleration to each EEG channel separately, on a mathematically robust and sample adaptive basis. This means that for each sample of data recorded, a modified (cleaned) signal is outputted from our algorithm. We leveraged the advantages of sample-adaptive non-linear projections to identify and remove the motion artifacts simultaneously.

The need for a tool that can handle complex non-linear characteristics of the motion artifacts is further justified by Figure 14. We have calculated the Spearman correlation coefficient between the vertical head acceleration and the raw EEG, complementing Figure 9. Note that the Spearman correlation gives meaningful results only when the relationship between two signals are monotonic. Nevertheless, notable similarities between the FC3, C2, F6 and F7 electrodes between the vertical-acceleration/EEG and vertical-

accelerations/identified-artifacts suggest that our method is capable of handling the monotonic non-linear relationship between the two signals, as well as handling the non-monotonic non-linearities as seen in Figure 9 power spectral plots.

The Volterra series expansion is not the most computationally efficient way of representing the non-linearities. However, we believe that there is a good tradeoff between the performance and computational load, as we have used a 2nd order representation, with 3 input signals. Our implementation (in Matlab C-MEX) on a Windows PC with dual 2,39 GHz processors is able to handle the cleaning of EEG data, from all 60 electrodes locations in real-time, with a safety margin of 6 times the real-time recording rate. For users looking for even faster processing can use the embedded coding version of our algorithm, or utilize a multi-threading approach, at least electrode-wise. Another alternative is to use the bilinear filter representation instead of the Volterra representation with somewhat reduced performance as discussed in [23]. Another option can be the use of reduced number of spectral target peaks. We have used all the identified spectral peaks as calculated from the IMU sensor, however one can also use every second (or nth) spectral peak, by choosing the bandwidth of the filter bank member to capture the overlapping frequencies.

For the dual purpose of this paper, that is, characterizing in detail the motion artifacts and introducing our method as a solution to the motion artifact problem, we have focused on targeted applications and frequency ranges that most suffer from the motion artifacts. We have not done any prior processing (except for in the loop cleaning of ocular artifacts and signal biases and drifts) to clean the muscle artifacts, electrode pops, and other physiological or non-physiological artifacts. Rather our implementation is intended to assess the level and characteristics of the motion artifacts alone, and clean them accordingly. Paired with our ocular artifact cleaning method, we have formed a unified framework for real-time filtering of two of the major EEG contaminants. We have limited our efforts to the 0.3-15 Hz range as the visible motion artifact harmonics were below 15 Hz for all walking speeds (Figure 5). Also muscle artifacts exist starting from ~20 Hz range, contaminating higher frequencies [25]. To represent our method's performance, we had to limit our efforts to a frequency range that ensures a specific contamination type, and targeted implementation for the motion artifact problem. For implementations that require higher frequency ranges, one could include the frequencies of the expected motion artifact harmonic spectral peaks into the cascade cleaning loop. We believe that there is no limitation for an effective cleaning of motion artifacts for the higher frequency ranges.

Moreover, our proposed method can be generalized to other types of artifacts, including fMRI gradient, fMRI Ballistocardiographic, EEG artifacts due to Transcranial Alternative Current Stimulation (tACS), to be presented elsewhere.

Acknowledgements

The authors would like to acknowledge the support of Mission Connect – A TIRR Foundation, NINDS award RO1NS075889 and NSF award 1827769. Authors also acknowledge the contributions of Kevin Nathan for helping with running the experimental paradigm.

References

- [1] K. Nathan and J. L. Contreras-Vidal, "Negligible motion artifacts in scalp electroencephalography (EEG) during treadmill walking," *Front. Hum. Neurosci.*, vol. 9, p. 708, 2016.
- [2] A. S. Oliveira, B. R. Schlink, W. David Hairston, P. König, and D. P. Ferris, "A channel rejection method for attenuating motion-related artifacts in EEG recordings during walking," *Front. Neurosci.*, vol. 11, no. APR, pp. 1–17, 2017.
- [3] J. E. Kline, H. J. Huang, K. L. Snyder, and D. P. Ferris, "Isolating gait-related movement artifacts in electroencephalography during human walking," *J. Neural Eng.*, vol. 12, no. 4, 2015.
- [4] A. S. Oliveira, "Induction and separation of motion artifacts in EEG data using a mobile phantom head device Induction and separation of motion artifacts in EEG data using a mobile phantom head device," *J. Neural Eng.*, vol. 13, no. 3, pp. 1–14, 2016.
- [5] K. L. Snyder, J. E. Kline, H. J. Huang, and D. P. Ferris, "Independent Component Analysis of Gait-Related Movement Artifact Recorded using EEG Electrodes during Treadmill Walking," *Front. Hum. Neurosci.*, vol. 9, no. December, pp. 1–13, 2015.
- [6] E. R. Symeonidou, A. D. Nordin, W. D. Hairston, and D. P. Ferris, "Effects of cable sway, electrode surface area, and electrode mass on electroencephalography signal quality during motion," *Sensors (Switzerland)*, vol. 18, no. 4, pp. 1–13, 2018.
- [7] A. F. Jackson and D. J. Bolger, "The neurophysiological bases of EEG and EEG measurement: A review for the rest of us," *Psychophysiology*, vol. 51, no. 11, pp. 1061–1071, 2014.
- [8] E. Niedermeyer, F. L. Da Silva, E. Niedermeyer, and F. H. Lopes Da Silva, *Electroencephalography: Basic Principles, Clinical Applications, and Related Fields*. Philadelphia, UNITED STATES: Wolters Kluwer, 2004.
- [9] J. T. Gwin, K. Gramann, S. Makeig, and D. P. Ferris, "Removal of Movement Artifact From High-Density EEG Recorded During Walking and Running," *J. Neurophysiol.*, vol. 103, no. 6, pp. 3526–3534, 2010.
- [10] E. Arad, R. P. Bartsch, J. W. Kantelhardt, and M. Plotnik, "Performance-based approach for movement artifact removal from electroencephalographic data recorded during locomotion," *PLoS One*, vol. 13, no. 5, pp. 1–15, 2018.
- [11] B. H. Kim, J. Chun, and S. Jo, "Dynamic motion artifact removal using inertial sensors for mobile BCI," in *2015 7th International IEEE/EMBS Conference on Neural Engineering (NER)*, 2015, pp. 37–40.
- [12] A. Bertrand, V. Mihajlovic, B. Grundlehner, C. Van Hoof, and M. Moonen, "Motion artifact reduction in EEG recordings using multi-channel contact impedance measurements," *2013 IEEE Biomed. Circuits Syst. Conf.*,

- pp. 258–261, 2013.
- [13] V. Mihajlovic, S. Patki, and B. Grundlehner, “The impact of head movements on EEG and contact impedance: An adaptive filtering solution for motion artifact reduction,” *2014 36th Annu. Int. Conf. IEEE Eng. Med. Biol. Soc. EMBC 2014*, pp. 5064–5067, 2014.
- [14] K. T. Sweeney, S. F. McLoone, and T. E. Ward, “The Use of Ensemble Empirical Mode Decomposition With Canonical Correlation Analysis as a Novel Artifact Removal Technique,” *Ieee Trans. Biomed. Eng.*, vol. 60, no. 1, pp. 97–105, 2013.
- [15] K. T. Sweeney, H. Ayaz, T. E. Ward, M. Izzetoglu, S. F. McLoone, and B. Onaral, “A methodology for validating artifact removal techniques for physiological signals,” *IEEE Trans. Inf. Technol. Biomed.*, vol. 16, no. 5, pp. 918–926, 2012.
- [16] K. Sweeney, “Motion Artifact Processing Techniques for Physiological Signals,” National University of Ireland Maynooth, 2013.
- [17] A. Kilicarslan, R. G. Grossman, and J. L. Contreras-Vidal, “A robust adaptive denoising framework for real-time artifact removal in scalp EEG measurements,” *J. Neural Eng.*, vol. 13, no. 2, p. 26013, 2016.
- [18] Y. Ye, Y. Cheng, W. He, M. Hou, and Z. Zhang, “Combining Nonlinear Adaptive Filtering and Signal Decomposition for Motion Artifact Removal in Wearable Photoplethysmography,” *IEEE Sens. J.*, vol. 16, no. 19, pp. 7133–7141, 2016.
- [19] H. M. Matsuzaki, “Adaptive Second-Order Volterra Filtering Based on an H infinity Criterion,” *SICE J. Control. Meas. Syst. Integr.*, vol. 9, no. 1, pp. 26–32, 2016.
- [20] B. Hassibi, T. Kailath, and S. Ca, “H infinity Adaptive Filtering,” *IEEE Int. Conf. Acoust. Speech Signal Process.*, pp. 949–952, 1995.
- [21] K. T. Sweeney, T. E. Ward, and S. F. McLoone, “Artifact removal in physiological signals—practices and possibilities,” *IEEE Trans. Inf. Technol. Biomed.*, vol. 16, no. 3, pp. 488–500, 2012.
- [22] C. Guerrero-mosquera and A. N. Vazquez, “Automatic Removal of Ocular Artifacts from EEG Data using Adaptive Filtering and Independent Component Analysis,” *17th Eur. Signal Process. Conf.*, no. Eusipco, pp. 2317–2321, 2009.
- [23] P. S. R. Diniz, *Adaptive Filtering-Algorithms and practical implementation*, vol. 39, no. 1. 1992.
- [24] J. T. Gwin, K. Gramann, S. Makeig, and D. P. Ferris, “Electrocortical activity is coupled to gait cycle phase during treadmill walking,” *Neuroimage*, vol. 54, no. 2, pp. 1289–1296, 2011.
- [25] S. Muthukumaraswamy, “High-frequency brain activity and muscle artifacts in MEG/EEG: a review and recommendations,” *Front. Hum. Neurosci.*, vol. 7, p. 138, 2013.